Geophys. J. Int. (2005) **160,** 1020–1026 doi: 10.1111/j.1365-246X.2005.02562.x

Hunting for oceanic island Moho

Garrett M. Leahy[1] and Jeffrey Park[1]

[1] *Yale University, Department of Geology and Geophysics,* PO Box 208109, *New Haven,* CT 06520-8109*, USA*

Accepted 2004 December 14. Received 2004 November 29; in original form 2004 June 14

SUMMARY

The structure of the oceanic crust conforms in general to a very simple model. However, fine-scale variations of this structure in anomalous regions (such as beneath oceanic islands) remain poorly resolved. Here we examine teleseismic receiver functions (RFs) computed at four permanent broadband seismic stations on islands in the Pacific region. The RF method is ideal for examining the fine structure of the crust because it is sensitive to the interfaces between layers, though less sensitive to average wave speed. RFs at these oceanic island stations are characterized by a train of *Ps* conversions from shallow depths, rather than the isolated Moho conversion typically seen at continental stations. We find that a simple three-layer structure (the old oceanic crust sandwiched between an extruded volcanic layer and an underplated layer) explains the main features of the RFs. Our data indicate that oceanic islands share a common structure, a principal feature of which is crustal underplating, with a total crustal thickness of 11–20 km.

Key words: oceanic crust, seismology, underplating, volcanic structure.

1 INTRODUCTION

Though the general properties of the oceanic crust are well known (e.g. Mutter & Mutter 1993; White *et al.* 1992), there are many details that remain unresolved. These details include fine structure underneath anomalous regions, such as oceanic islands. It is critical to understand the crustal structure in these regions, not least because they host many permanent seismic stations in ocean basins. The principal goal of this study is to investigate the crustal structure under several oceanic island stations using teleseismic receiver functions (RFs). For this purpose, we consider the seismic stations RAR (Rarotonga, Cook Islands), PPT (Tahiti, Society Islands), XMAS (Kiribati, Line Islands) and POHA (the island of Hawaii) (Fig. 1). These stations were chosen due to their broad geographical distribution and the availability of broadband seismic data.

Previous studies of crustal thickness underneath oceanic islands (e.g. Caress *et al.* 1995; Grevemeyer & Flueh 2000; McNutt & Bonneville 2000; Wolfe *et al.* 1994) have found evidence for crustal underplating in the Pacific. An underplated layer lies beneath preexisting crust, and exhibits seismic velocities lower than expected for the mantle but higher than expected for the crust. Crustal underplating is often inferred to occur as a by-product of plume–lithosphere interaction, a mafic intrusion from which oceanic island basalts are derived. We evaluate evidence for this phenomenon at the islands we consider, to determine if this is merely a local feature or a widespread characteristic of hotspots in general.

Conventional wisdom tells us that seismic data from oceanic island stations are noisy and must be used with great caution. In addition, arrivals of converted phases from interfaces near the surface arrive very close to the direct arrival and may be difficult to detect. Nevertheless, signals can be extracted with careful data processing. Using the method of Park & Levin (2000), we compute RFs with multiple-taper cross-correlation (MTC). The multiple-taper RF operates in the frequency domain, allowing practical application at the higher frequencies demanded by the shallow oceanic interfaces.

A simple model for crustal structure would predict a clean and easily identifiable *Ps* conversion from the Moho as seen at continental stations. However, a more sophisticated model for oceanic island crustal structure including possible underplating and extruded volcanics would predict a more complicated RF trace. In this paper we show how failure to represent oceanic island RFs with a simple crust led us to hypothesize a crustal model containing three layers (a volcanic layer, the old oceanic crust and an underplated layer) to explain the main characteristics of observed RFs at four permanent mid-ocean seismic stations. We do not parametrize very fine-scale layers in the old oceanic crust associated with marine refraction studies (sediment, pillow basalts and gabbros). We also ignore fine structure in the volcanic layer (such as subaerially extruded layers and those extruded above water).

Resolution of fine layering is limited by the need to reconstruct two closely spaced *Ps* converted waves from the top and bottom of a distinct layer. If both *Ps* pulses have identical polarity, resolution is limited by the relation $H = (p_{PS} f)^{-1}$ where H is the layer thickness, f is the frequency of the receiver function and $p_{PS} = v_s^{-1} - v_p^{-1}$ is the differential slowness of the *Ps* converted phase. For igneous crustal lithologies, $p_{PS} \approx 0.125$, so that $f = 8$ Hz must be resolved in the RF to retrieve $H = 1$ km layering. Because multiple-taper RF processing involves a tapered cut-off in the frequency domain,

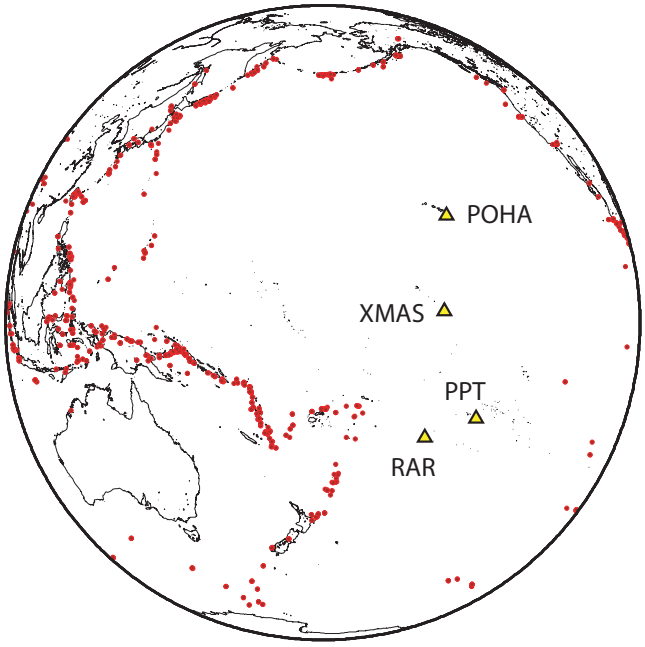

Figure 1. The Pacific Ocean. Plotted are stations (triangles) and events (circles) considered in this study.

the nominal frequency cut-off f_c of the MTC RF should be at least 30 per cent greater than the frequency one wishes to resolve. Resolution of a low-velocity layer is more forgiving, because the *Ps* converted phases from its upper and lower interfaces have opposite polarity, and therefore can be distinguished by half of a seismic period.

2 DATA ANALYSIS

We compiled 491 teleseismic *P* codas, of which 166 were recorded at RAR, 182 at PPT, 67 at XMAS and 76 at POHA. Seismic events were selected based on epicentral distance ($\Delta > 20^\circ$), magnitude (6.3 M_s or greater), signal-to-noise ratio and availability. The majority of the data fall into the range $50^\circ < \Delta < 90^\circ$. A broad variety of backazimuths are present, though there are some gaps due to the geometry of the Pacific Plate.

We compared RFs with cut-off frequencies f_c between 2.5 and 5 Hz (3 Hz shown in the figures) at each station. When stacked and plotted versus epicentral distance, the bin-averaged RFs have a striking coherence. The averaging scheme uses a 10° moving window to compute an average RF every 5° (for both backazimuth and epicentral presentations). This means that RF traces separated by at least 10° are independent. The RFs at POHA, PPT, RAR and XMAS all share similar features on the radial component (Figs 2, 3, 4, 5, 6, 7, 8 and 9): a train of sharp positive-amplitude pulses arriving within the first 4 s (at all stations) which we attribute to *Ps* conversions from crustal layers. These are followed by a complex crustal reverberation, mostly with negative amplitude. At low frequencies (less than 1 Hz), our RFs agree with a recent study by Li *et al.* (2003). However, accurate identification of converted phases is difficult at these low frequencies.

The transverse RFs also demonstrate similar consistency, both versus epicentral distance and between stations. Polarity flips on the transverse components correlate with some interfaces proposed below, and perhaps may indicate anisotropic lithology.

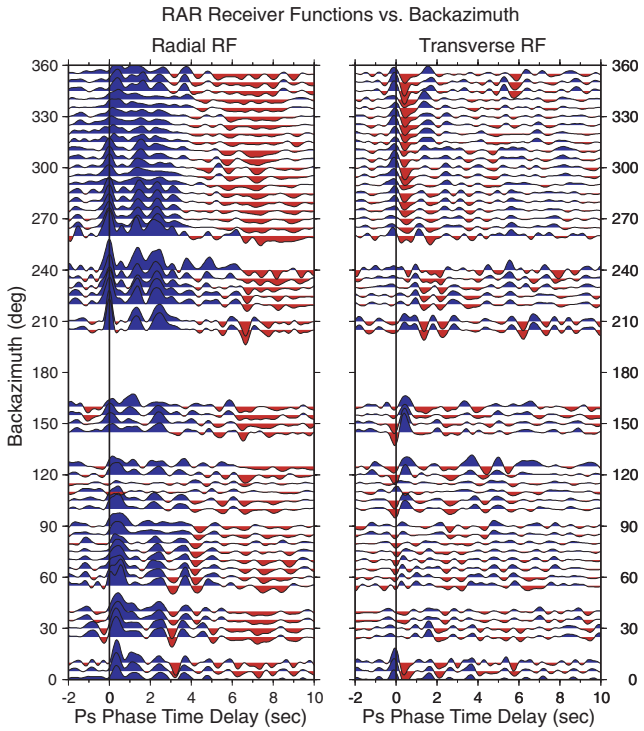

Figure 2. Radial and transverse receiver functions for RAR (Rarotonga). The RFs are plotted versus backazimuth for an epicentral range $50^\circ < \Delta < 90^\circ$. Individual RFs from each event are averaged using a 10° moving window centred every 5°. This means that RF traces separated by 10° contain independent data.

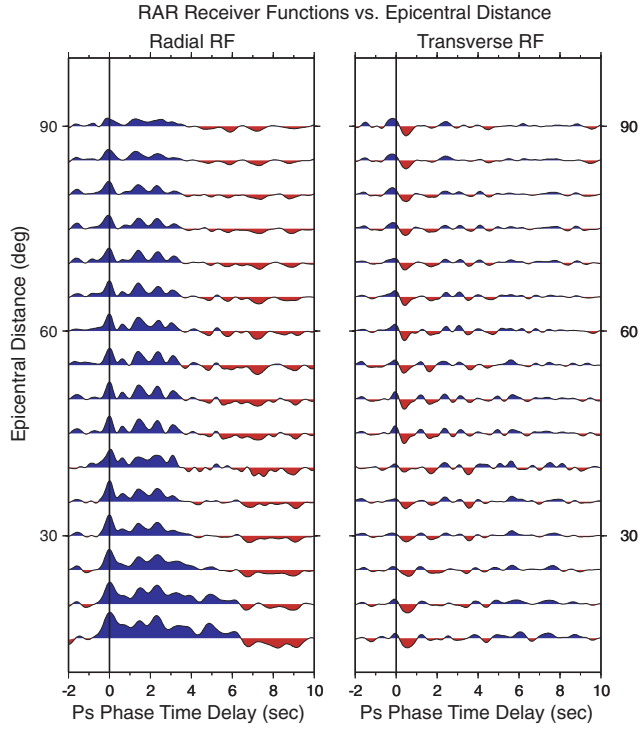

Figure 3. Radial and transverse receiver functions for RAR (Rarotonga). The RFs are plotted versus epicentral distance for a backazimuth range 265°–300°. Individual RFs from each event are averaged using a 10° moving window centred every 5°. This means that RF traces separated by 10° contain independent data.

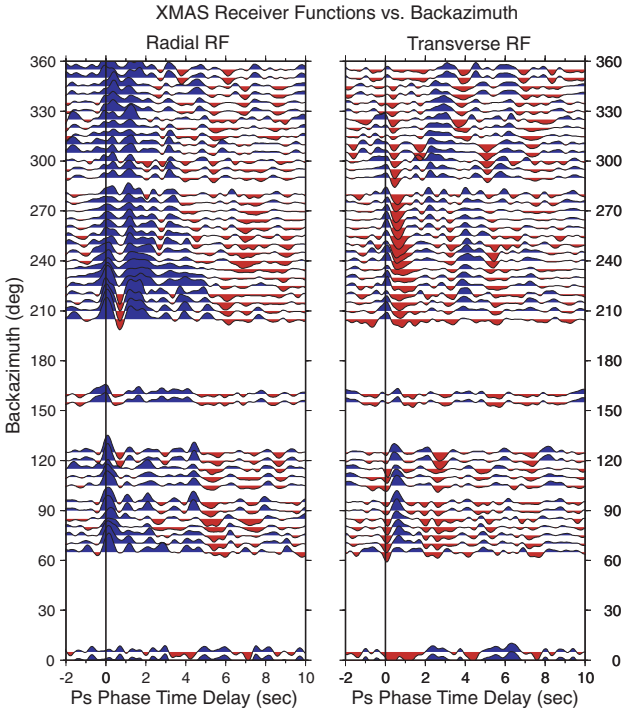

Figure 4. Radial and transverse receiver functions for XMAS (Kiribati). The RFs are plotted versus backazimuth for an epicentral range $50^\circ < \Delta < 90^\circ$. See Fig. 2 for stacking details.

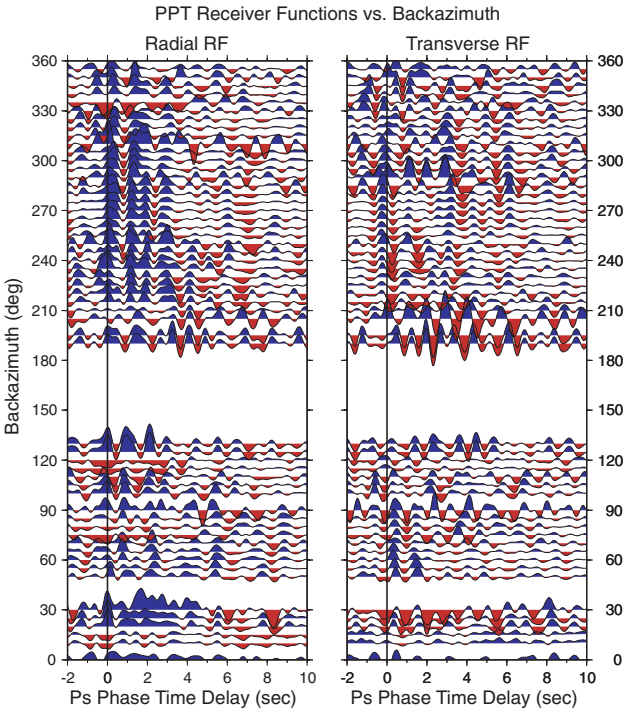

Figure 6. Radial and transverse receiver functions for PPT (Tahiti). The RFs are plotted versus backazimuth for an epicentral range $50^\circ < \Delta < 90^\circ$. See Fig. 2 for stacking details.

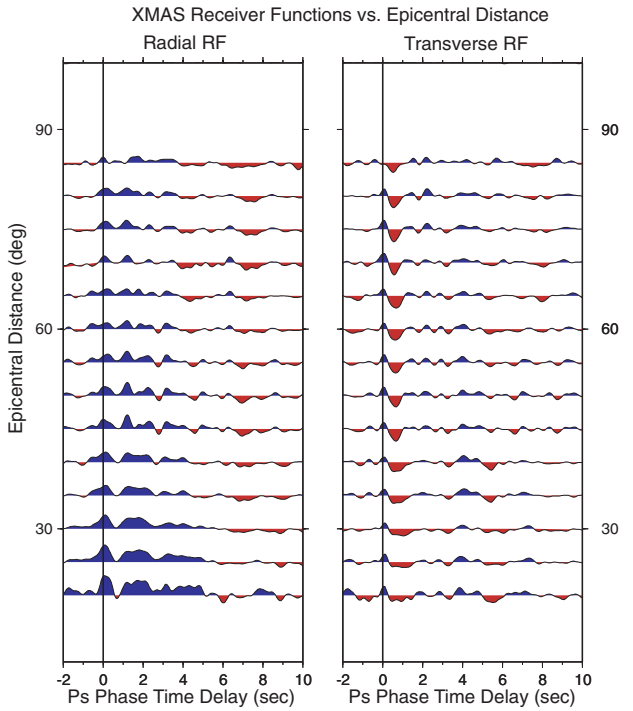

Figure 5. Radial and transverse receiver functions for XMAS (Kiribati). The RFs are plotted versus epicentral distance for a backazimuth range 225°–270°. See Fig. 3 for stacking details.

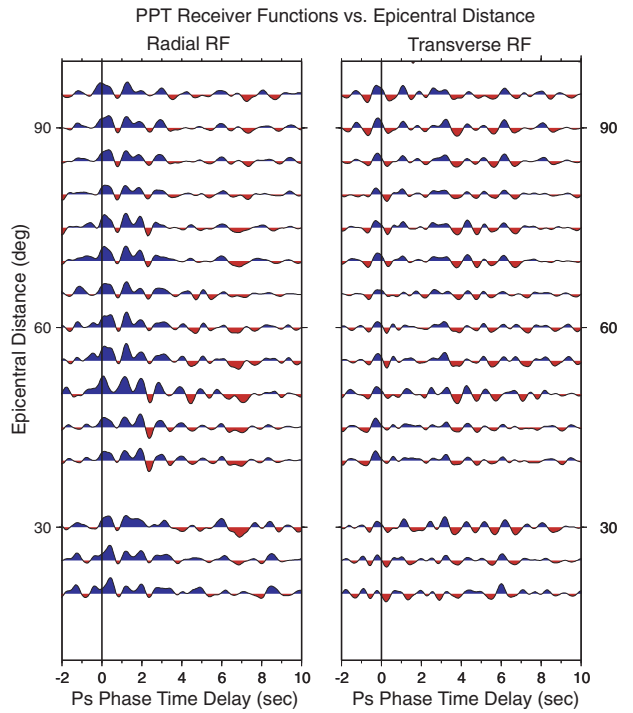

Figure 7. Radial and transverse receiver functions for PPT (Tahiti). The RFs are plotted versus epicentral distance for a backazimuth range 265°–300°. See Fig. 3 for stacking details.

3 RESULTS

In order to focus the interpretation of our results, we first used the stacking method of Zhu & Kanamori (2000) to guide our calculations of crustal thickness. This method sums the contributions of four different phases (*Ps*, *PpPs*, *PpSs* and *PsPs*) in the RFs at times predicted by a simple single-layer geometry. The optimal layer thickness and v_p/v_s ratio are chosen to be those which

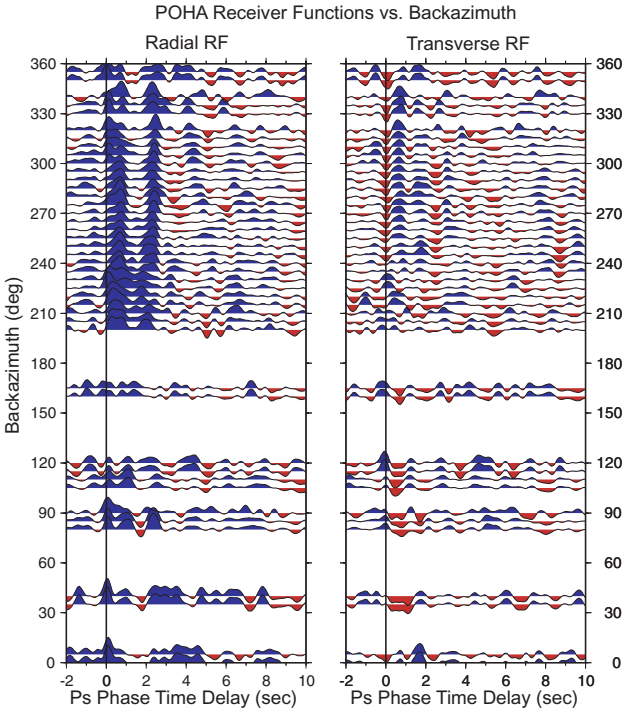

Figure 8. Radial and transverse receiver functions for POHA (Hawaii). The RFs are plotted versus backazimuth for an epicentral range $50^\circ < \Delta < 90^\circ$. See Fig. 2 for stacking details.

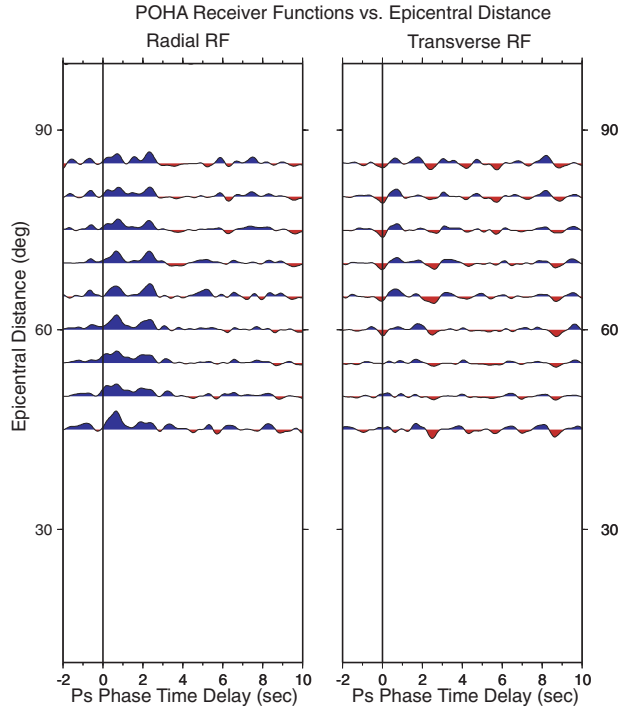

Figure 9. Radial and transverse receiver functions for POHA (Hawaii). The RFs are plotted versus epicentral distance for a backazimuth range 225°–270°. See Fig. 3 for stacking details.

maximize the stacking. However, we found that for the oceanic stations, varying the v_p/v_s ratio has little effect on the predicted crustal thickness. The inferred layers are too thin to constrain the velocities using this technique.

In addition, the application of the Zhu and Kanamori method to our RFs assuming a single-layered crust resulted in three different solutions for crustal thickness. This indicates the presence of three well-defined interfaces below the surface with physical differences (potentially compositional or fabric related) significant enough to spawn *Ps* conversions. We interpret this result to indicate three primary layers in the crust under islands (Fig. 10): a volcanic layer extruded on top of normal (old) oceanic crust, both of which are underlain by a layer of underplated material.

Using this slightly more sophisticated model for crustal structure, we attempt to fit the predicted arrival times of 10 direct and reverberated phases in the crust. Because the Zhu and Kanamori method yielded poor constraints on layer velocity, we parametrized our model using the crustal velocities of Crust2.0 (Laske *et al.* 2003) for the old oceanic crust, gabbroic velocities for the underplated layer (7.1 km s^{-1}, Mutter & Mutter 1993), and typical extruded basalt velocities for the volcano (4.5 km s^{-1}, Watts *et al.* 1985). We set the shear velocity for the volcanic layer to be 2.9 km s^{-1}, calibrated from fitting the first-arriving *Ps* delay to estimated local bathymetry. Though our choices for v_p do not alleviate the ambiguity associated with velocity versus layer thickness trade-offs, we can use this model to estimate layer thickness. We performed a grid-search in three variables (the thicknesses of the three layers) for the structure that minimizes the predicted arrival times of the phases with pulses observed in the data. The RF traces that we attempt to fit are the station averages for all events between 50° and 60° epicentral distance. Most features in these station-averaged RF are visible over broad sectors of backazimuth in the bin-averaged RF sweeps, which lends some support to our interpretation of them

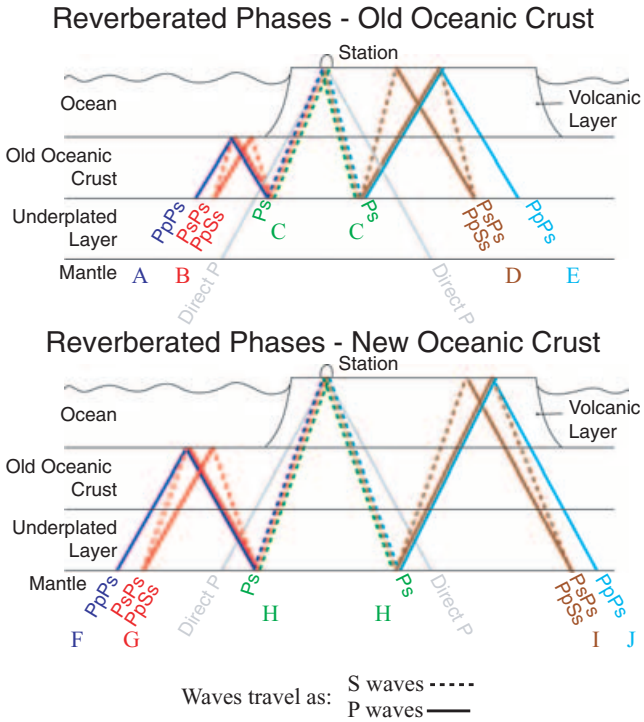

Figure 10. Modelled phases. Our model for the crust under oceanic islands is composed of three layers: a volcanic layer, the old crust and an underplated layer. We model the travel times of 10 phases in this study. Phases A–E are *Ps* conversions and reverberations in the top two layers—the old oceanic crust and the volcanic layer. Phases F–J are *Ps* conversions and reverberations in the whole crust. Phases diagrammed correspond to phases identified in Fig. 11.

as *Ps* reverberations. However, a 1-D model for *Ps* reverberations beneath a 3-D oceanic island is far from ideal, so the accuracy of our models of layer thickness is probably poorer than formal error analysis would suggest.

3.1 Rarotonga (RAR)

Previous seismic studies in the Cook Islands (Hochstein 1967) did not directly observe crustal thickness under Rarotonga. However, they found at a nearby island a crust of standard thickness (6.4 km) underlain by what was reported as 'anomalously slow upper mantle' with *P*-wave velocity less than 7.7 km s^{-1}. We interpret this to be indicative of an underplated layer rather than slow upper mantle.

Using traveltime constraints, we identify the first three pulses in the RAR RFs as direct *Ps* conversions from the base of the volcano, the base of the old crust (old Moho) and the base of the underplated layer (Moho) (Fig. 11c). In addition, a fourth positive-amplitude phase appears to be a reverberation in the old oceanic crust. Subsequently arriving phases are less clear, but *Ps* polarity in the data appears to match the theoretical predictions (blue positive; red negative). For Rarotonga, we find that the data are best fitted by a 5 km thick volcanic layer, 6 km of old crust and 8 km of underplated material (Fig. 12c).

3.2 Kiribati (XMAS)

The Kiribati RFs show structure that resembles RFs estimated for Rarotonga (Fig. 11d). The XMAS data cannot, however, be interpreted in an identical fashion. The *Ps* conversion from the base of the volcano is not readily apparent in the range of epicentral distances considered (50° and 60°) as it cancels in the RF averaging. Because we can identify the 'volcano' pulse in RFs averaged over narrow sectors of backazimuth, we attempt to fit the data with a volcanic layer that equals the ocean depth. A layer structure with a 4.5 km volcano, 4.5 km of old oceanic crust and a 5 km underplated layer (Fig. 12d) fits the direct *Ps* conversions and reverberated phases. If we were to (mistakenly) identify the first visible positive *Ps* pulse as from the base of the volcano, we would infer that an 8 km volcanic layer is required, and the arrival times of reverberated phases would not correspond to those seen in the RFs.

3.3 Tahiti (PPT)

Crustal thickness underneath Tahiti was found to be 13 km by Patriat *et al.* (2002), confirming previous refraction studies (e.g. Talandier & Okal 1987). Talandier & Okal (1987) model the crustal structure as a 4.2 km thick volcanic layer underlain by 8.8 km of oceanic crust. Grevemeyer *et al.* (2001) argue that late-stage volcanics in the region have modified the lower crust and may contribute to underplating.

Similar to station XMAS, the station-average RF traces do not show a *Ps* conversion from the bottom of the volcano, though a *Ps* with variable polarity and time delay $\tau < 1$ s is visible in the RFs averaged over narrow backazimuth sectors. If we do not take this variable-amplitude *Ps* as the base of the volcano, PPT would require an extruded layer that is over 8 km thick in order to interpret the first station-averaged *Ps* conversion as from the volcano's base. This is not consistent with local bathymetry. We found that the predicted timing of direct and reverberative *Ps* phases are best matched by the station-averaged PPT RFs if we assume a volcanic layer thickness comparable to local bathymetry (Fig. 11a). The results of our analysis yield a thin old oceanic crust (3 km) and a thin underplated layer

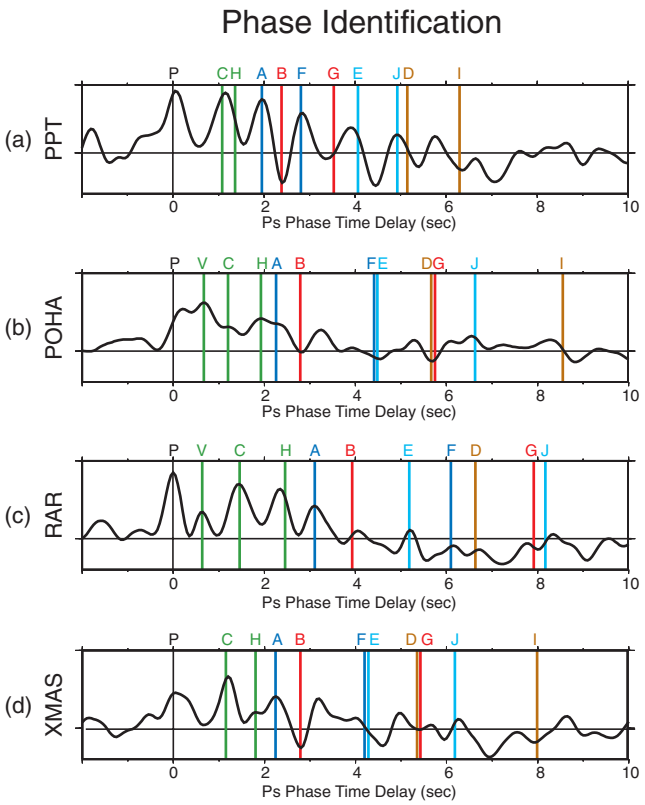

Figure 11. Phase identification (for a diagram of modelled phases see Fig. 10). Shown are RF averages for all events between 50° and 60° epicentral distance at each station. (a) PPT. The first three positive amplitude pulses are identified as *Ps* conversions from the bottom of the old crust and the underplated layer (arriving together, C and H), a *PpPs* phase reflecting off the sea floor (in the top two layers, A), similar phase that travels through all three layers (F). The first negative amplitude pulse corresponds to *PsPs* and *PpSs* phases arriving together (B). Though not apparent in this RF trace, other RF traces at PPT contain a *Ps* conversion from the base of the volcano. (b) POHA. In this RF we can identify *Ps* conversions from the bottom of each layer (V, volcano; C, old crust; H, underplated layer), and subsequent reverberated phases. (c) RAR. In this RF we can identify *Ps* conversions from the bottom of each layer (V, volcano; C, old crust; H, underplated layer), and subsequent reverberated phases. (d) XMAS. We do see a clear *Ps* conversion from the base of the lower two layers. The *Ps* conversion from the base of the volcano (V) does not appear on this averaged RF; however, it is visible in other records.

(3 km) (Fig. 12a). The velocity trade-off could be used to create a two-layer model similar to that of Talandier & Okal (1987), where the bottom layer is just the standard, old oceanic crust. A model of this type would then have to explain why a mid-crustal interface (such as between layer 2 and layer 3 type materials) would result in such strong *Ps* conversions. In either case, our total predicted crustal thickness of about 11 km approaches the results of previous researchers.

3.4 Hawaii (POHA)

Studies underneath the Hawaiian Islands have proposed the existence of a subcrustal plutonic unit (Watts *et al.* 1985), though subsequent studies have yet to provide conclusive evidence for this (e.g. ten Brink & Brocher 1987; Watts & ten Brink 1989; Lindwall 1988). Under the island of Hawaii, James & Savage (1990) predicted a crustal thickness of 13–14 km from seismic reflection data.

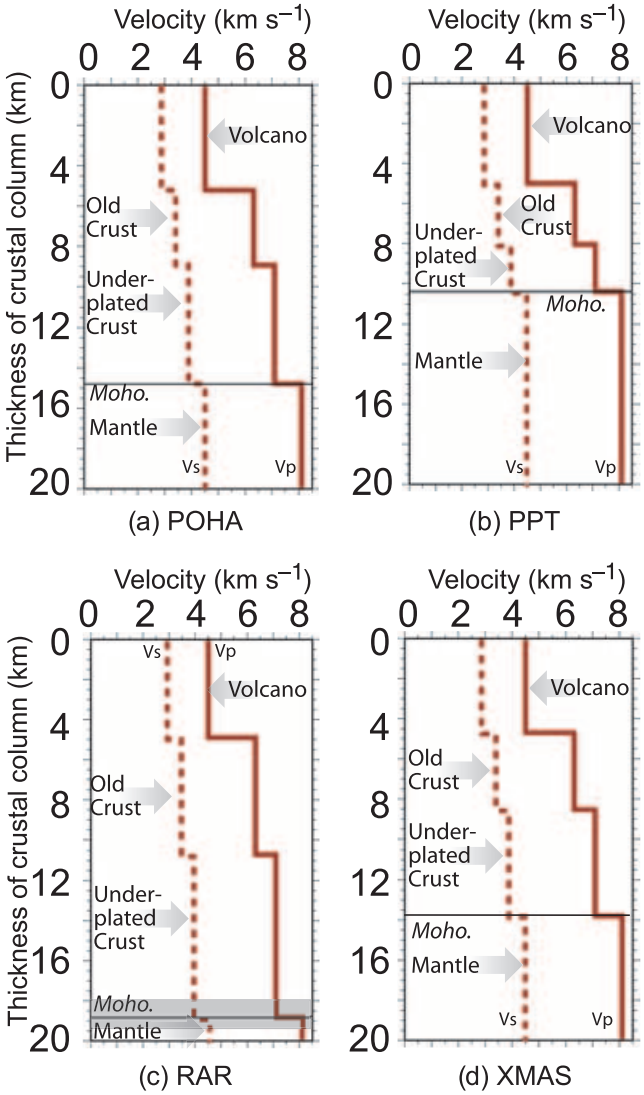

Figure 12. Preferred models of crustal thickness at (a) PPT (11 km), (b) POHA (15 km), (c) RAR (19 km), (d) XMAS (14 km). At RAR, the estimated range of thicknesses for the underplated layer based on the uncertainty in the velocity of the underplated layer is represented by the grey shaded area (c).

A receiver function study was recently completed (Li *et al.* 2004) at POHA that found the lithosphere under the island to be thermally rejuvenated.

Though the data from POHA do not appear initially to show the same pulse-train features as the other three islands, careful modelling identifies the same four phases seen at RAR: *Ps* conversions from the base of the volcano, the old ocean crust and the Moho, as well as a reverberated phase in the old crust (Fig. 11b). The more complex reverberations are not modelled as well as at RAR, which may be an indication of significant topography on the interfaces. Our simple model considers only flat layers, though one clearly would anticipate flexure in the underlying plate due to loading and buoyancy forces (e.g. ten Brink & Brocher 1987; Watts & ten Brink 1989; Lindwall 1988) to complicate this issue. Also, the differences could be due to the fact that our model neglects the sediment layer at the ocean floor (underneath the extruded volcanic layer), which could have a large effect on the impedance contrast at the base of the volcano and thus the seismic signature. The station POHA is far from the Kilauea volcano, and therefore the receiver functions should not be affected by the magma body there.

Our preferred model predicts a total crustal thickness of about 15 km, which is in fairly good agreement with previous studies (Fig. 12b). This is composed of a large volcanic layer (almost 6 km—POHA is located at 2 km elevation above sea level) a thinner (4 km) old crust and about 5 km of underplated material.

4 SUMMARY

Our preferred crustal model underneath the stations of POHA, PPT, RAR and XMAS consists of three dominant crustal waveguides: an extruded volcanic layer, the original Pacific crust and new underplated crust. Oceanic island receiver functions are defined principally by *Ps* conversions from the base of each layer and by a series of complex reverberations in this layer.

Our model leads to total crustal thicknesses that correlate well with other studies but do depend on the input velocity model. Our conservative use of Crust 2.0 (Laske *et al.* 2003) allows us to image the general characteristics of these islands, but more accurate estimates will require better knowledge of lower crustal velocity (particularly shear velocity) structure. More representative shear velocities for the volcanic layer (v_p/v_s of about 1.8) result in smaller volcanic layers. This could be due to the fact that the lower portions of the volcano, though above the ocean floor, are primarily characterized by intrusive volcanism. The interface we interpret as the base of the volcano would then correlate with the transition from intrusive to extrusive igneous rock. In our model, this would require a thin volcanic layer and a thicker 'old crust' layer to compensate.

More sophisticated waveform modelling would place greater constraints on layer velocities. However, this type of analysis would need to address the effects of likely anisotropic velocity jumps between layers. Variations in *Ps* amplitude and polarity are strong indicators of anisotropy beneath the four hotspot islands in this study. (Because anisotropy resides in layers of thicknesses of 10 km or less, its influence on shear wave splitting is likely to be negligible.) Additionally, better constrained velocities would not significantly influence the results of our analysis. This can be shown by a simple estimate of the uncertainty in our model layer thicknesses due to the velocity trade-off. At Rarotonga, we vary the velocity of the lower layer to span a range of previous observations (6.5–7.5 km s^{-1} Mutter & Mutter 1993). This results in thickness variations in the underplated layer from 7.7 to 9.1 km (Fig. 12c, shaded region).

It is interesting to note that the 19 km thick crust at RAR does not correspond to a significant surface swell as is seen at other islands. Though previous results from the Marquesas (McNutt & Bonneville 2000) show that the chemical effects of underplating can reproduce the bathymetric swell far from the volcanic edifice, it seems unlikely that our observations could be associated with the hotspot and yet have no surface expression. This may indicate that underplating is not necessarily limited to an island's immediate neighbourhood, but instead extends more broadly in the old Pacific.

ACKNOWLEDGMENTS

This work was supported by NSF grant OPP-0136191. Vadim Levin, Michael Ryan and two anonymous reviewers offered useful comments on this project. We obtained seismic data from the Data Management Center of the Incorporated Research Institute for Seismology (IRIS). Stations RAR, XMAS and POHA are maintained by

the IRIS Global Seismographic Network, and station PPT is maintained by Project Geoscope. We used GMT software (Wessel & Smith 1995) to prepare many figures.

REFERENCES

Caress, D., McNutt, M., Detrick, R. & Mutter, J., 1995. Seismic imaging of hotspot-related crustal underplating beneath the Marquesas Islands, *Nature,* **373,** 600–603.

Grevemeyer, I. & Flueh, E., 2000. Crustal underplating and its implications for subsidence and state of isostasy along the Ninetyeast Ridge hotspot trail, *Geophys. J. Int.,* **142,** 643–649.

Grevemeyer, I., Weigel, W., Schussler, S. & Avedik, F., 2001. Crustal and upper mantle seismic structure and lithospheric flexure along the Society Island hotspot chain, *Geophys. J. Int.,* **147,** 123–140.

Hochstein, M., 1967. Seismic measurements in the Cook Islands, south-west Pacific Ocean, *N. Z. J. Geol. Geophys.,* **10,** 1499–1526.

James, D. & Savage, M., 1990. A search for seismic reflections from the top of the oceanic crust beneath Hawaii, *Bull. seism. Soc. Am.,* **80**(3), 675–701.

Laske, G., Masters, G. & Reif, C., 2003. *Crust 2.0: A Global Crustal Model at 2 × 2 Degrees,* http://mahi.ucsd.edu/Gabi/rem.html

Li, X., Kind, R. & Yuan, X., 2003. Seismic study of upper mantle and transition zone beneath hotspots, *Phys. Earth planet. Int.,* **136,** 79–92.

Li, X., Kind, R., Yuan, X., Wolbern, I. & Hanka, W., 2004. Rejuvenation of the lithosphere by the Hawaiian plume, *Nature,* **427,** 827–829.

Lindwall, D., 1988. A two-dimensional seismic investigation of crustal structure under the Hawaiian islands near Oahu and Kauai, *J. geophys. Res.,* **93**(B10), 12 107–12 122.

McNutt, M. & Bonneville, A., 2000. A shallow, chemical origin for the Marquesas swell, *Geochem. Geophys. Geosyst.,* **1,** doi:1999GC000028.

Mutter, C. & Mutter, J., 1993. Variations in thickness of layer 3 dominate oceanic crustal structure, *Earth planet. Sci. Lett.,* **117,** 295–317.

Park, J. & Levin, V., 2000. Receiver functions from multiple-taper spectral correlation estimates, *Bull. seism. Soc. Am.,* **90**(6), 1507–1520.

Patriat, M. *et al.,* 2002. Deep crustal structure of the Tuamotu Plateau and Tahiti (French Polynesia) based on seismic refraction data, *Geophys. Res. Lett.,* **29**(14), 1.

Talandier, J. & Okal, E., 1987. Crustal structure in the Society and Tuamotu Islands, French Polynesia, *Geophys. J. R. astr. Soc.,* **88,** 499–528.

ten Brink, U. & Brocher, T., 1987. Multichannel seismic evidence for a subcrustal intrusive complex under Oahu and a model for Hawaiian volcanism, *J. geophys. Res.,* **92**(B13), 13 687–13 707.

Watts, A. & ten Brink, U., 1989. Crustal structure, flexure, and subsidence history of the Hawaiian islands, *J. geophys. Res.,* **94**(B8), 10 473–10 500.

Watts, A., ten Brink, U., Buhl, P. & Brocher, T., 1985. A multichannel seismic study of lithospheric flexure across the Hawaiian-Emperor Seamount chain, *Nature,* **315,** 105–111.

Wessel, P. & Smith, W., 1995. New version of the generic mapping tools released, *EOS, Trans. Am. geophys. Un.,* **76,** 329.

White, R., McKenzie, D. & O'Nions, R., 1992. Oceanic crustal thickness from seismic measurements and rare earth element inversions, *J. geophys. Res.,* **97,** 19 683–19 715.

Wolfe, C., NcNutt, M. & Detrick, R., 1994. The Marquesas archipelagic apron: Seismic stratigraphy and implications for volcano growth, mass wasting, and crustal underplating, *J. geophys. Res.,* **99**(B7), 13 591–13 608.

Zhu, L. & Kanamori, H., 2000. Moho depth variation in southern California from teleseismic receiver functions, *J. geophys. Res.,* **105**(B2), 2969–2980.